POST PRINT
https://www.sciencedirect.com/science/article/pii/S0162013415301057
https://doi.org/10.1016/j.jinorgbio.2015.10.014.

Viviana Vergaro, Paride Papadia, Stefano Leporatti, Sandra A. De Pascali, Francesco P. Fanizzi, Giuseppe Ciccarella, Synthesis of biocompatible polymeric nano-capsules based on calcium carbonate: A potential cisplatin delivery system, Journal of Inorganic Biochemistry,Volume 153, 2015, 284-292

Synthesis of biocompatible polymeric nano-capsules based on calcium carbonate: a potential *cisplatin* delivery system

Viviana Vergaro[a], Paride Papadia[b]*, Stefano Leporatti[a], Sandra A. De Pascali[b], Francesco P. Fanizzi[b], and Giuseppe Ciccarella[a,b]*

[a] CNR NANOTEC-Istituto di Nanotecnologia - CNR, Via Arnesano, 73100 Lecce, Italy.

[b] Dipartimento di Scienze e Tecnologie Biologiche ed Ambientali, Università del Salento, Via Monteroni 73100 Lecce, Italy

[*] Corresponding authors.

Email addresses: paride.papadia@unisalento.it (P. Papadia),

giuseppe.ciccarella@unisalento.it (G. Ciccarella).

Abstract

A smart nanocarrier system for cancer therapy, based on a recently developed technique for preparing pure nanometric calcium carbonate ($CaCO_3$), was studied. Different approaches were used to obtain sustained release of *cisplatin*: at first, pure $CaCO_3$ nanoparticles were evaluated as carriers, then the nanoparticles were functionalized with polymer or silanes, and finally they were employed as a substrate to build layer by layer (LbL) self-assembled polyelectrolyte nanocapsules. Loading efficiency and release kinetics were measured. The best loadings were obtained with the LbL nanocapsules, allowing for high loading efficiency and the possibility of controlling the release rate of the drug. The behavior of all the carriers was evaluated on four neoplastic cell lines, representative of different types of neoplastic disease, namely MCF-7 (breast cancer), SKOV-3 (ovarian cancer), HeLa (cervical cancer) and CACO-2 (human epithelial colorectal adenocarcinoma). Negligible cytotoxicity of the nanoparticles, functionalized nanoparticles, and nanocapsules was observed in experiments with all cell lines. Nanocapsules were functionalized with fluorescein isothiocyanate (FITC) in order to track their kinetic of internalization and localization in the cell line by confocal laser scanning microscopy (CLSM). The cytotoxicity of the loaded capsules was evaluated, showing cell survival rates close to those expected for non encapsulated *cisplatin* at the same nominal concentration.

Keywords: drug delivery, calcium carbonate nanoparticles, Layer-by-Layer, *cisplatin*

1. Introduction

Nano-sized drug carriers like polymer conjugates, liposomes, micelles, dendrimers, inorganic or other solid particles, and many others brought important contributions to cancer therapy over the last decade.[1, 2] Advantages of such nanocarriers lie in their ability to improve drug solubility, prolong systemic drug half-life, provide means for sustained and environmentally responsive drug release, enable tumor specific delivery, reduce immunogenicity and systemic side effects, suppress development of drug resistance and also deliver simultaneously two or more drugs for combined therapy.[3]

Among the large variety of nano/microparticles described in literature and optimized to increase efficacy and improve the delivery into cancer cells, one can find calcium carbonate ($CaCO_3$). Calcium carbonate is an extremely important biomaterial whose behavior is driven by its defined proprieties, such as morphology, structure, size, specific surface area and chemical purity. In our previous work we demonstrated that calcium carbonate microparticles can be considered an ideal drug carrier due to their excellent biocompatibility and ability to readily penetrate cancer cells.[4] Furthermore they allowed us to engineer microcapsules of polyelectrolytes multilayers starting from calcium carbonate micro-core templates, capable to encapsulate various classes of drug molecules, by using polymers that are biodegradable or that can respond and release their payload in response to well-defined stimuli.[5-7] To respond to the requirements of the biomedical field to delivery anti-tumor drugs, we have developed a smart method for the synthesis of particles of calcium carbonate of nanometric dimensions. This spray drying method allows to synthesize pure and thermodynamically stable nano calcium carbonate by a fast and atom economic method.[8] The technique is easily scalable allowing at the same time to tune the size and morphology without surfactants or other chemical species commonly used to stabilize the mixture and the reaction product.

In this work the nanometric $CaCO_3$ is used as both template and as direct carrier to load the most widely used platinum-based anti-neoplastic agent, *cis*-dichloro diammineplatinum(II) (*cis*-$[PtCl_2(NH_3)_2]$, *cisplatin*).[9] It is a potent drug that is usually administered intravenously for treatment of solid malignancies.[10] Apart from its well established clinical value, it is one of the few approved transition-metal-based drug, inspiring generations of inorganic chemists to pursue application of their research in medical sciences.[11] However, a major obstacle to more widespread use of *cisplatin* is the persistence of severe toxic side effects.[12] Other disadvantages associated with *cisplatin* clinical use include short circulation period in the blood due to glomerular excretion,[13] intrinsic or acquired resistance of some tumors to the drug and limited aqueous solubility (1.0 mg/mL).[14] *Cisplatin* undergoes ligand exchange reactions kinetics which are largely determined by the nature of the leaving groups. In biological fluids *cisplatin* can react irreversibly with a variety of nitrogen- and sulphur-containing biomolecules that reduce its therapeutic concentration.[15, 16] However, *cisplatin* also reacts with weaker nucleophiles, *i.e.* carboxylate ions, and the resulting species are able to undergo the reverse exchange reaction with chloride ions to regenerate *cisplatin* at physiological salt concentrations. It is estimated that up to 90% of *cisplatin* binds to plasma proteins,[17] and as low as 1% of intracellular *cisplatin* manages to actually interacts with DNA[18, 19] to give the intrastrand cross-links between adjacent purines,[20] the lesions considered to be responsible[21] for the antitumoral activity. Creating a drug delivery system able to reduce the drug loss on the way could and targeting the cell would therefore be a dual advantage. We have investigated several ways to load the *cisplatin* into systems based on $CaCO_3$. The results reported demonstrated how the loading efficiency can be changed exploiting the calcium carbonate features, functionalizing their surface by silane, covering it with polymers in order to create a capsule.[6] The latter strategy was the one that gave the best results. The polymeric nanocapsules were obtained according the layer by layer technique (LbL), a method used widely to fabricate hollow multilayered capsules by depositing

polyelectrolytes onto cores afterwards sacrificed after film formation.[22-31] The majority of polyelectrolyte capsules described in literature are composed of pairs of synthetic not biodegradable polymers (*e.g*. polystyrenesulfonic acid and polyallylamine hydrochloride, PSS and PAH), or composed of biocompatible and biodegradable (*e.g*. protamine and dextran sulfate, PRM and DXS) polymers, which are more suitable to medical therapy. Of the two pairs of polyelectrolytes we selected, PRM/DXS and protamine/alginate (PRM/ALG), the best loading efficiencies were obtained with the latter.

2. Experimental Section

2.1. Chemicals

The following reagents were used (abbreviations, if used, and source in parentheses): dextran sulfate sodium salt from Leuconostoc s (DXS, Sigma, USA), protamine sulfate salt, grade III (PRM, Sigma, USA), polystyrenesulfonate sodium salt (PSS, Sigma, USA), alginic acid sodium salt (ALG, Sigma, USA), calcium chloride dehydrate 99.99% ($CaCl_2$•$2H_2O$, Aldrich, USA), sodium hydrogen carbonate ($NaHCO_3$, pro analysis, Merck, Germany), ethylenediaminetetraacetic acid disodium salt 99+% (EDTA, Sigma, USA), fetal bovine serum (FBS, Sigma, USA), penicillin-streptomycin solution (Sigma, USA), sodium pyruvate (Sigma, USA), DMEM medium (Sigma, USA), [4,5-dimethylthiazol-2-yl]-2,5- diphenyl tetrazolium bromide ≥ 97.5% TLC (MTT, Sigma, USA), phosphate buffer solution, Dulbecco A (PBS, Oxoid), sephadex G25 (Sigma, USA), fluorescein isothiocyanate, isomer I (FITC , Aldrich, USA).

2.2. Synthesis of nano-$CaCO_3$

Pure $CaCO_3$ nanoparticles were synthesized by an atomization process[8], which involves the mixing of two aqueous solutions: $NaHCO_3$ and $CaCl_2$ at molar ratio 2:1 (**Scheme 1**). The reaction is carried out in atmosphere and temperature-controlled.

$$2NaHCO_3 + CaCl_2 \rightarrow 2NaCl + Ca(HCO_3)_2$$

$$Ca(HCO_3)_2 \rightarrow CaCO_3 + H_2O + CO_2$$

Scheme 1. Chemical reaction

The two solutions are mixed using two pumps which allow a fine control of flow rate of each reagents. Then they are atomized in a hot air flow at 140°C. The high temperature causes a rapid evaporation of the reaction mixture water, and allows the direct production of the powder of calcium carbonate and of sodium chloride, which are accumulated in a collection vessel; the reaction by-product (NaCl) can be easily removed by means of later water washings.

2.3. Silane modification of nano-$CaCO_3$

A minimal amount of anhydrous ethanol was added to the nano-calcium carbonate power. Then, the mixture was ultrasonic dispersed for 30 min. Under vigorous magnetic-stirring at 30°C, 0.75 mL silane (Aminopropyltriethoxysilane, APTES, methyltrimethoxysilane MTMS or methyltriethoxysilane MTES) solution was added drop wise. After stirring at 30°C for another 5 h, the mixture was centrifuged at 4000 rpm/min for 15 min to separate the APTES, MTMS, or MTES modified nano-calcium carbonate from the reaction medium. Finally, the silane modified nano-calcium carbonate was washed with ethanol for 5 times, dried at vacuum and kept for application.

2.4. Capsules Fabrication

Polyelectrolyte nanocapsules were prepared by alternating incubation of $CaCO_3$ nanoparticles in DXS and PRM aqueous solutions (2.0 mg mL^{-1}), or in ALG and PRM solutions (2.0 mg

mL^{-1}). The pH of the polymer solutions was adjusted to 6.5 by addition of HCl/NaOH. Capsules were fabricated in a two-step procedure. In a first step, the $CaCO_3$ nanoparticles were coated by using a LbL technique. 1.0 mg of powder of $CaCO_3$ were dispersed in a solution containing the polyanion (DXS or ALG). The dispersion was continuously shaken for 10 min. The excess polyanion was removed by three centrifugation/washing steps with deionized water. Thereafter, 1.0 mL of solution containing the polycation (PRM) was added and the dispersion was continuously shaken for 10 min, followed again by three centrifugation/washing steps. This procedure was repeated several times for each polyelectrolyte resulting in the deposition of four or six polyelectrolyte layers on the $CaCO_3$ particles. Coated colloids were cross-linked by 0.5% glutaraldehyde (GA) at room temperature (20-25°C) for 30 minutes followed by three centrifugation/washing steps. In a second step, the $CaCO_3$ core was removed by complexation with EDTA. Cross-linked coated particles were shaken for 2 min with 1.0 mL of a 0.2M EDTA solution pH 5.5 was adjusted by HCl, followed by centrifugation and redispersion in 1.0 mL of a fresh EDTA solution pH 7.5. The hollow nanocapsules obtained in this way were washed four times with deionized water and stored at 4°C in water. To fabricate capsules with fluorescent-labeled polyelectrolytes, the same procedure was used with DXS-FITC. In order to study the localization and internalization of these nanoparticles, polymeric colloids of nano-$CaCO_3$ nanoparticles were prepared using a couple of synthetic polyelectrolytes, PSS and PAH-FITC.

2.5. Transmission Electron Microscopy (TEM)

TEM images were recorded with a Jeol Jem 1011 microscope operated at an accelerating voltage of 100 kV. We prepared samples for analysis by dropping a dilute nanoparticles dispersion in water onto carbon-coated copper grids and then allowing water to evaporate.

2.6. Cell culture

MCF-7 (human breast cancer), HeLa (human cervical cancer), SKOV-3 (human ovarian cancer), and CACO-2 (human epithelial colorectal adenocarcinoma) cell lines were used. Cancer cell lines were maintained in DMEM medium supplemented with FBS (10%), penicillin (100 U/mL culture medium), streptomycin (100 µg/mL culture medium), glutamine (5%). Cells were grown in a humidified incubator at 37°C, 5% CO_2, and 95% relative humidity. Cell lines were serum-starved for 24h before any test.

2.7. Cytotoxicity assays

All cell lines were used in the general cytotoxicity test. The MTT system measuring the activity of living cells via mitochondrial dehydrogenase activity. The key component is 3-[4,5-dimethylthiazol-2-yl]-2,5- diphenyl tetrazolium bromide or MTT. Mitochondrial dehydrogenases of viable cells cleave the tetrazolium ring, yielding purple MTT formazan crystals which are insoluble in aqueous solutions. Naked or functionalized $CaCO_3$, at the concentration of 1mg/mL, or *cisplatin* loaded-capsules suspension, at a concentration of 0.5 mg/mL, was diluted with complete culture medium. The MTT method of cell determination is most effective when cultures are prepared in multiwall plates. Cells (10^5 cells/mL) were added to 24-well culture plates at 1000 µL/well, serum-starved for 24h, and incubated at 37°C in 5% CO_2, 95% relative humidity for 48 hours with the microcapsules suspension. The control was a complete culture medium. After an appropriate incubation period, cultures were removed from incubator and a MTT solution in an amount equal to 10% of the culture volume was aseptically added. Cultures were returned to incubator and incubated for 3 hours. After the incubation period, cultures were removed from incubator and the resulting MTT formazan crystals were dissolved with dimethysulfoxide (DMSO). The plates were ready within 15 min. After the incubation time, pipetting up and down was required to completely dissolve the MTT formazan crystals. Absorbance at wavelength of 570 nm was spectrophotometrically

measured using the ELISA plate reader. Results were expressed as mean ± S.D. of three separate trials.

2.8. Confocal Laser-Scanning Fluorescence Microscopy (CLSM)

Laser scanning confocal microscopy was performed on a Zeiss LSM700 (Zeiss, Germany) confocal microscope equipped with an Axio Observer Z1 (Zeiss, Germany) inverted microscope using an objective 100×, with 1.46 numerical aperture oil immersion lens for imaging. Laser beams with 405, 488 and 542 nm excitation wavelengths were used for Hoechst, labeled nano-$CaCO_3$, and cytoskeleton, respectively.

Cancer cell lines ($5x10^4$) were seeded onto 35 mm glass bottom Petri Dish and incubated over-night. The cells were incubated with the fluorescent calcium carbonate nanoparticles for 3 hours in dark in a humidified incubator at 37°C, 5% CO_2, and 95% relative humidity. The cells were then rinsed with PBS, fixed with glutaraldehyde 0.25% and the images were examined under confocal microscope.

2.9. ζ-potential measurement

The electrophoretic mobility of the nanoparticles was measured by using a Malvern Nano ZS90 (Malvern Instruments, UK). The potential analysis of particles was carried out by Laser Doppler Velocimetry (LDV), with an appropriate sample dilution in ultra-pure water. Representative measurements of three distinct set of data have been reported ± S.D.

2.10. Uptake efficiency

The uptake efficiency was investigated according to J. Zhang, *et al.*[32] MCF-7, SKOV-3, HeLa and CACO-2 cells were transferred to 24-well culture plates (10^5 cells/mL). The culture medium was replaced by phosphate-buffered saline 1x (PBS, pH 7.4) and pre-incubated at 37°C for 30 minutes. After equilibration, cellular uptake of capsules was initiated by

exchanging the transport medium with capsules suspension 0.5mg/mL in PBS 1x and incubated at 37°C for different time point up to 2 hours. The experiment was terminated by washing the cells three times with 5 mL ice-cold PBS 1x, after which 0.1% Triton X-100 in 0.2 M NaOH solution was added to lyse the cells. Cell-associated FITC-capsules were quantified by analyzing the cell lysate in a fluorescence plate reader (λ_{ex} 485 nm, λ_{em} 528 nm). Uptake efficiency was then calculated by following formula:

$$\text{Uptake efficiency } (\%) = (W_{sample}/W_{total})*100$$

Where W_{sample} is the amount of FITC associated to cells, W_{total} is the amount of FITC associated to the initial suspension.

2.11. *Cisplatin* loading and quantification by inductively coupled plasma atomic emission spectroscopy (ICP)

Cisplatin (50 – 75 – 150 µM) was added to an aqueous solution containing naked or functionalized calcium carbonate nanoparticles, or polymeric nanocapsules, followed by stirring of the mixtures for 24h at room temperature. Unbound *cisplatin* was removed by dialysis against deionized water for 5 hours using membrane with MWCO 3500.

After washing and centrifugation, drug loading were calculated in the supernatant by ICP. For each concentration was constructed a calibration line, using 4 points for each line. Loading percentage is defined as the number of *cisplatin* ppt in solution after loading divided by the number of *cisplatin* ppt in solution before loading. [*cisplatin*] is defined as the initial concentration of *cisplatin*. ICP experiments were performed with Thermo Scientific iCap 600 series ICP-OES.

2.12. Release kinetics

The release kinetics was evaluated in phosphate buffer at physiological pH. The release experiments were performed using 0.5 mg of polymeric nanocapsules in 10 mL of phosphate

buffer saline solution (PBS, pH 7.4) at 37°C. The concentration used (0.5mg/10mL) was the same used in the cytotoxicity experiments. Polyelectrolytes capsules loaded with *cisplatin* were constantly stirred in order to increase the release rate and to establish equilibrium condition. Separate tubes were used for each time. At each time point, 500 µL release media was replaced with the same volume of fresh release media. At selected time intervals, loaded particles or capsules were separated by centrifugation. The supernatant was collected and the *cisplatin* content in the supernatant was determined by ICP analysis, according to a standard calibration curve of platinum.

3 Experimental Section

3.1 Synthesis and characterization of calcium carbonate nano-crystals

The crystalline phase obtained during synthesis of calcium carbonate can be influenced by other factors than temperature, such as surfactants, other ions and pH.[33-37] In the present case, the carbonate source used was $NaHCO_3$ instead of the more commonly used Na_2CO_3, creating a mildly basic environment in the droplets generated during the spray drying process. Homogeneous spherical nanoparticles of calcite (Powder X-ray diffraction patterns in **Fig. SM1**) could be produced by means of this synthetic technique. Morphological characterization was obtained by electron microscopy analysis.

As shown in tunnel electron microscopy (TEM) images (**Fig. 1** and **Fig. SM2**) the nanoparticles have an ellipsoidal shape. A statistical analysis of particles' size using 20 TEM images was performed, using the Image-J V1.49 software to measure 10 randomly sampled nanoparticles in each image, for a total of 200 size measurement. For each of the nanoparticles, major and minor diameter were separately measured. The average of measurements of major diameter was 93 ± 9 nm and the minor 35 ± 10 nm (average ± S.D. of all measurements).

During synthesis procedures high temperature causes a rapid evaporation of the reaction mixture water, and allows the direct production of the powder of calcium carbonate and of sodium chloride, which are accumulated in a collection vessel; the reaction by-product (NaCl) can be easily removed by means of later water washings.

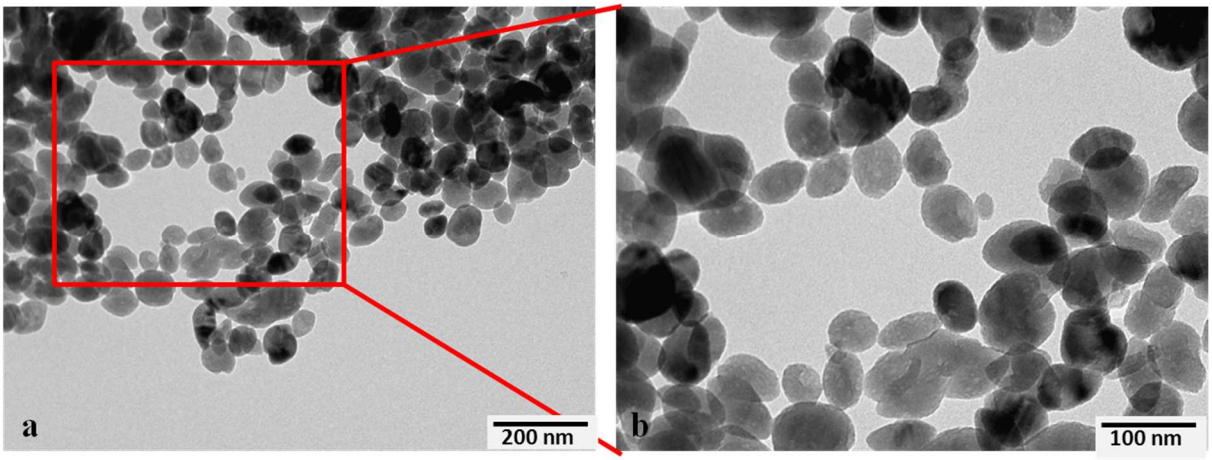

Fig. 1. (a) TEM characterization of nano$CaCO_3$ nanoparticles, (b) magnification of (a) image.

To check the stability of nanoparticles the ζ Potential was evaluated by means of electrophoretic light scattering (ELS). $CaCO_3$ nanoparticles were suspended in ultra-pure water, phosphate buffer saline (pH 7.4) or in culture medium.

The ζ-potential in function of pH was measured and nanoparticles surface charge was monitored at different pH (2−10) by adding 0.1 M HCl or NaOH to the suspension. As can be seen from the graph in **Fig. 2**, the surface charge of the nano-$CaCO_3$ shifts to positive side with the decrease in pH. This change in the potential is the result of the decrease in the carbonate ion concentration, [CO_2^-], caused by its protonation, *i.e.* the increase in the Ca^{2+} concentration.

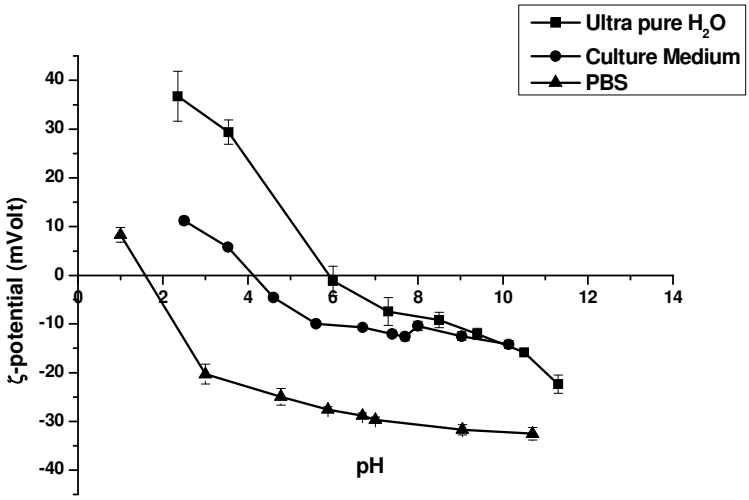

Fig. 2 Variation of ζ-potential of nano-$CaCO_3$ measured in different dispersant: (square) ultra-pure water, (circle) culture media and (triangle) PBS buffer. Averages of 3 separate measurements.

Furthermore, at a physiological pH of 7.4, the samples exhibited a good dispersion in ultra-pure water (222.7 nm ± 9.2 nm) and in PBS buffer (188.8 nm ± 4.4 nm) as suggested by the high polydispersity index (PDI) values (around 0.2-0.3). Bigger aggregates having a wide range of diameters (300-380 nm) were found in culture medium, with PDI values around 0.6-0.7 because of protein corona absorption.

3.2 Silane modification

Due to the large amount of hydroxyls (-OH) on the surface of nano-calcium carbonate, the –Si $(OCH_3)_3$ or $(OCH_2CH3)_3$ group of silanes hydrolyzes to silicon alcohol group (-SiOH) during coupling reactions. Then, silicon alcohol group reacts with the hydroxyls (-OH) on the powder surface to form hydrogen bonds, resulting in the formation of –SiO-M covalent bond (M represented $CaCO_3$ powder particle surface) due to dehydration and condensation. The silicon alcohols of different silane molecule associate with each other to form a membrane

with network structure. The membrane covers the surface of the powder, making the surface organized. Similarly, the chemical coupling reaction takes place between amino-silane coupling agent, APTES and –OH groups. Therefore, APTES molecules may be used to form outer amino functional groups on the outer surface of nano-calcium carbonate.

Three different silane coupling agents were used for nano-calcium carbonate surface modification, allowing successful preparation of nano-calcium carbonates with hydrophobic surface. TEM characterization (**Fig. 3**) showed that silane coupling agents were connected to the surface of nano-calcium carbonate enhancing its dispersion and separation.

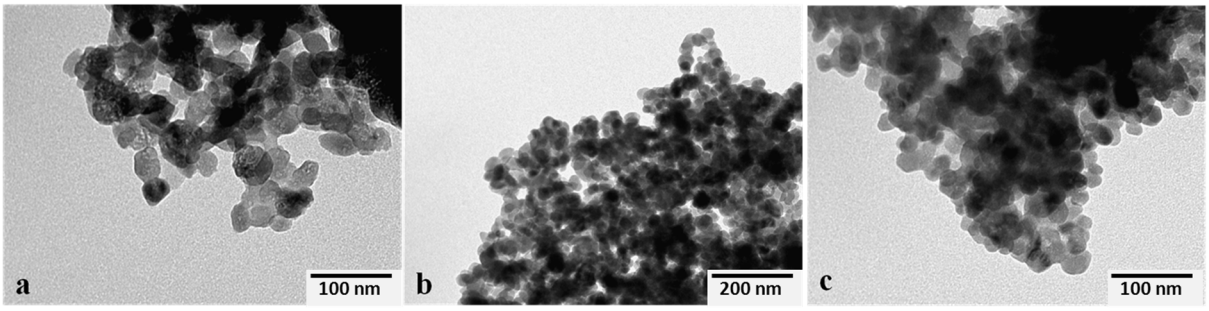

Fig. 3. TEM characterization of $CaCO_3$ nanoparticles after silane modification (a) APTES, (b) MTMS, (c) MTES

Nanoparticles maintained their shape and a good colloidal stability as confirmed by ζ-potential measurement reported in **Table 1**.

Table 1 ζ-potential characterization

Samples	**ζ-value ± SD (mVolt)**
$CaCO_3$	-9.4 ± 1.32
$CaCO_3$ APTES	-18.5 ± 0.6145
$CaCO_3$ MTMS	-20.2 ± 0.87
$CaCO_3$ MTES	-17.5 ± 0.98

3.3 Polymeric nanocapsules by LbL technique

As described in the experimental section LbL approach consists of alternate absorption of polyanions and polycations. Film growth is achieved stepwise by the repetitive exposure of substrates to sequential polycation and polyanion solutions. Positively charged substrates are immersed into the solution of a negatively charged polymer for several minutes. Consequently a polymeric thin layer of 1-2 nm thickness is adsorbed on the surface. The substrate is afterwards washed for removing not adsorbed material and placed into the polycation solution. This procedure can be repeated several times to reach a desired layer thickness defined by the number of coating cycles. This gives rise to multilayered films composed of alternate layers of polycations\polyanions. Their thickness depends on the number of layers deposited and the solution conditions (such as temperature, ionic strength, pH, etc.) used.[22, 38-41]

Properties and functionalities of hollow capsules can be tuned in the nanometer range by varying their wall features. The permeability changes in response to the ionic strength, solvent or pH.[24] After assembly of oppositely charged polyelectrolytes, the core is removed to obtain hollow capsules whose wall and inner cavity can be encapsulated and functionalized.[31] The produced hollow capsules usually have a wall thickness of a few tens up to several hundred nanometers and their diameter ranges depending on the size of the original core.

The deposition of each layer was checked by ζ-potential measurements (**Fig. 4**). The charge of nanoparticles change from negative (DXS and ALG) to positive (PRM) depending on the polyelectrolytes used.

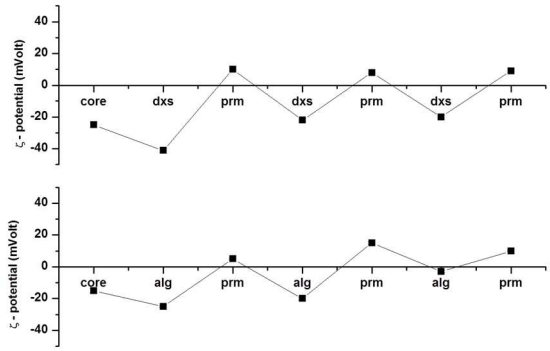

Fig. 4. ζ-potential measurements of two pairs of polyelectrolytes DXS/PRM, ALG/PRM

Crucial components for capsule fabrication are templates and polyelectrolyte pairs constituents. $CaCO_3$ is efficient material for templates because it is stable during coating, but can also be dissolved and completely removed from the interior of the capsules by treating it with mildly acidic aqueous solutions containing a cation chelating agent.

In this case, cross-linked coated colloids were shaken with an EDTA solution at pH 5.5 in order to remove the salt from the interior of the nanocapsules. The hollow capsules so obtained were washed four times with deionized water and stored at 4°C in ultra-pure water.

3.4 Cytotoxicity assessment

MTT assays were performed at different time intervals (24 to 48 to 72 h) and at different concentrations (from 1.0 μg/mL up to 1.0 mg/mL) with naked calcium carbonate (data not shown). The cell viability was preserved at 100% and confirmed the biocompatibility of material. The biocompatibility test was additionally performed for the three silane functionalized nano-$CaCO_3$ (**Fig. 5**), but not for the capsules, since the biocompatibility of polymeric capsules was already established in our previous works.[4-6]

The powder (1.0 mg/mL maximum concentration) was dispersed in the culture medium and then added to the cell cultures. MCF-7, SKOV-3, HeLa, and CACO-2 cells were used. The

results shown in the figure demonstrates that silane functionalization does not affect the material's biocompatibility, with viability values around 98% in all cancer cell lines. These results are consistent with those obtained for other inorganic nanoparticles like Fe_3O_4[42], when APTES is used as surface modifiers or cross linker, with the specific functional group having negligible impact on cell survival.

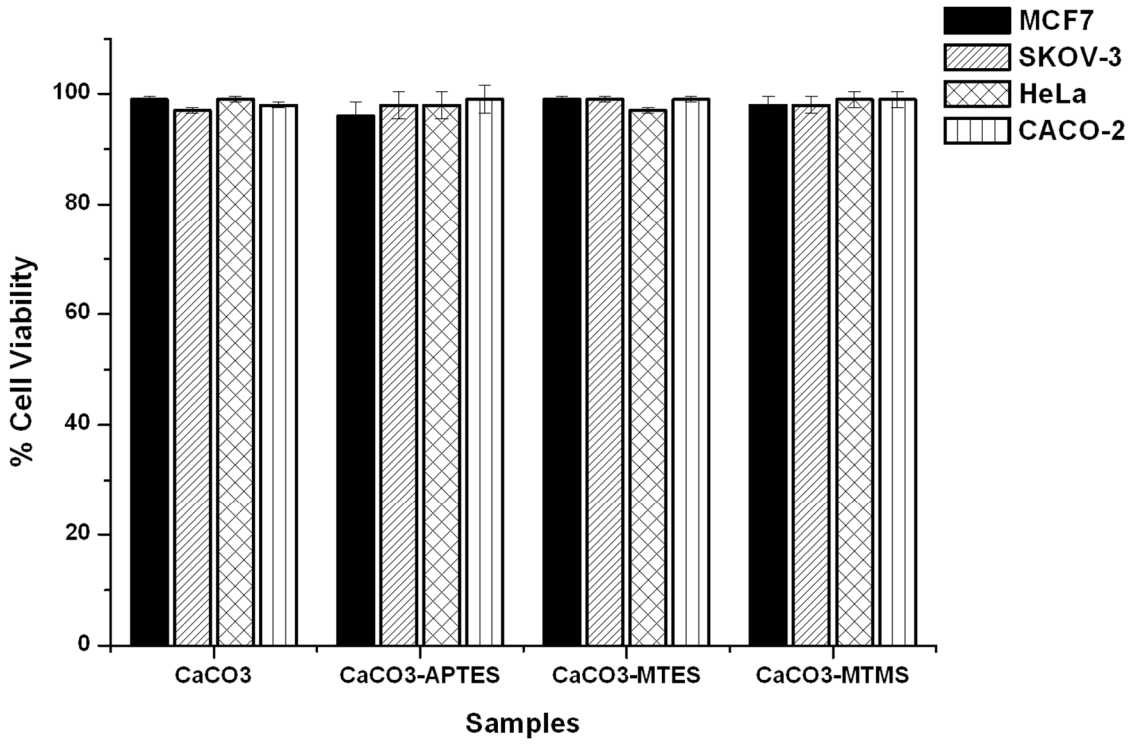

Fig. 5. Cell Viability test performed on MCF7, SKOV-3, HeLa and CACO-2 cell lines incubated for 24h with 1mg/mL of naked $CaCO_3$ or silane functionalized $CaCO_3$.

3.5 Internalization of coated particles

Cisplatin and the related FDA-approved platinum-based drugs operate by similar mechanisms of action. These agents kill cancer cells by binding to nuclear DNA.[43, 44] The process by which such compounds do so involves several steps, of which cellular uptake is the first. The efficacy of a platinum anticancer agent depends upon its ability to enter the cell and penetrate the nucleus where the critical target, DNA, resides. Much research has been devoted to

elucidating the pathways by which *cisplatin* is internalized by cells.[45] Once inside the cell, *cisplatin* becomes activated by aquation, the substitution of chloride ligands by water. This reaction gives rise to the potent electrophilic cations *cis*-$[Pt(NH_3)_2Cl(OH_2)]^+$ and *cis*-$[Pt(NH_3)_2(OH_2)_2]^{2+}$.

According to previous reports by others groups which indicated that capsules are internalized by living cells despite to their large size, allowing us to expect the same behavior.[27, 46] Thanks to their nanometer size and positive superficial charge, internalization by cancer cells was in fact observed. For studying their localization and digestion, cancer cell lines were cultured for 3 hours in the presence of synthetic not biodegradable PSS/PAH nano-$CaCO_3$. The cellular internalization was confirmed by using MCF-7, SKOV-3, HeLa and CACO-2 cells, with FITC labelled nanoparticles being dosed at a constant particle mass (0.5 mg/mL). The kinetics of particle internalization was evaluated by using the fluorescence method. Cell-associated FITC-nanoparticles were quantified by analyzing the cell lysate in a fluorescence.

The time course of particle internalization was studied from 5 min up to 3 h (**Fig. 6**).

To minimize the possible interference of the residual capsules externally bound to the cells, a PBS solution was used to wash extensively the cells after incubation. The possibility of residual nanocapsules adsorbed on the cell membrane can't be completely excluded, but the confocal fluorescence microscopy experiments performed in parallel to the cell lysis showed that the fluorescence was localized inside the cells only (**Fig. 7**).

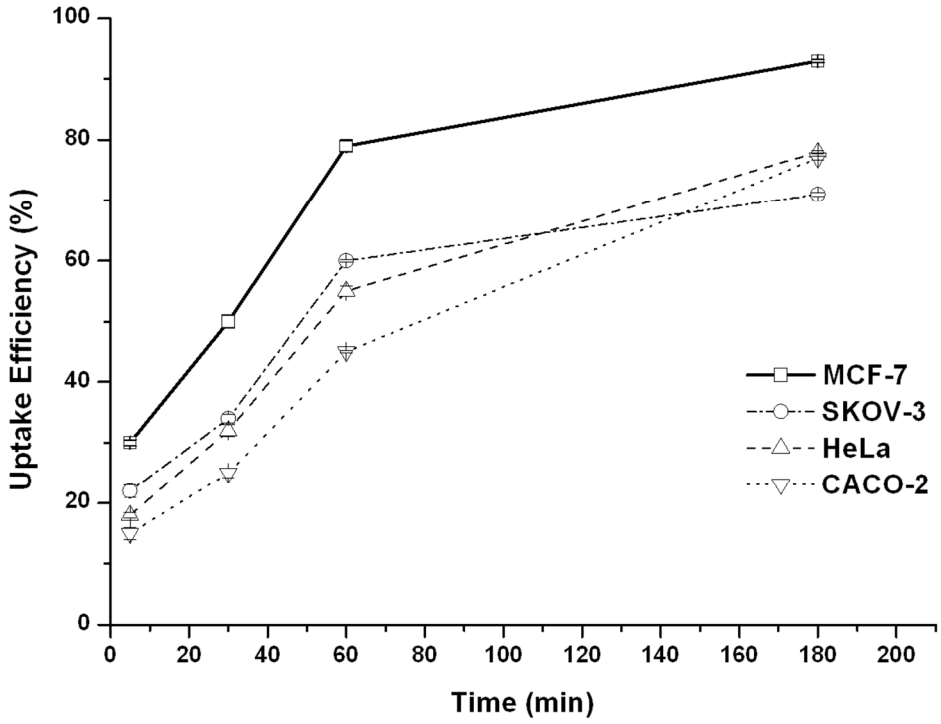

Fig. 6. Kinetics for the uptake of nanoparticles by MCF-7, SKOV-3, HeLa, and CACO-2 cells measured by fluorescence spectroscopy.

Coated colloids were spontaneously uptaken by cancer cells. As shown, the kinetics is dependent on the kind of cell lines. In MCF-7 cells after 3 hour almost complete internalization was reached (around 95%), slightly faster than other cell lines. HeLa and CACO-2 cells reached a peak 75% of internalization after 3 hours of incubation, the SKOV-3 cell line showed the least amount of FITC associated with cells at the same time.

For visualizing their uptake and to assess colloids intracellular fate, only one of polyelectrolytes used for coating (labeled as PAH-FITC) was conjugated with fluorescein moieties. In particular, all cells were incubated with non biodegradable PSS/PAH nanoparticles since the synthetic multilayer is not enzymatically degraded by proteases. The localization of PSS/PAH coated nanoparticles in these cells lines was found to be perinuclear, as indicated by white arrows in **Fig. 7** and in selected Z-stack sections in **Fig. 8**.

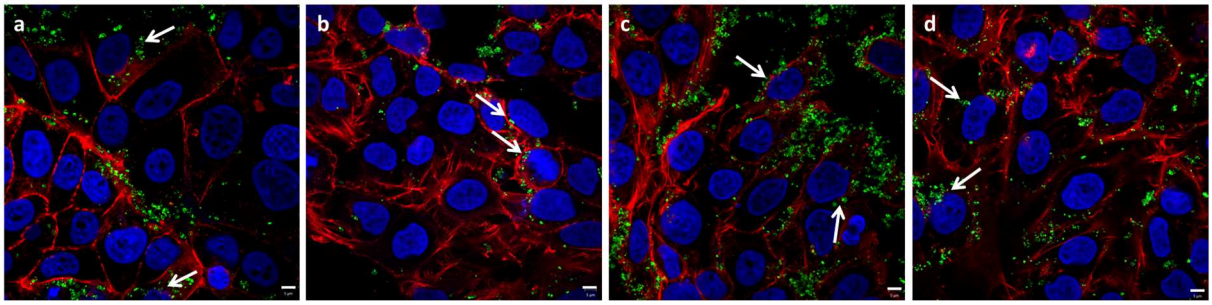

Fig. 7. Confocal microscopy images of nano$CaCO_3$ uptake by MCF-7 (a) SKOV-3 (b), HeLa (c) and CACO-2 (d). In blue are stained nuclei, in red the cytoskeleton (phalloidin-TRITC) and in green nano-$CaCO_3$. Scale bar 5µm.

The size of the FITC-fluorescent spots suggest that noticeable aggregation of the nanoparticles occurs inside the cells. No layer removal\degradation upon cell contact\interaction was detected and the majority of capsules were digested spontaneously externally near to nuclear region. PSS/PAH coated colloids remained still intact as fluorescent nanoparticles upon 3 hours from cell uptake.

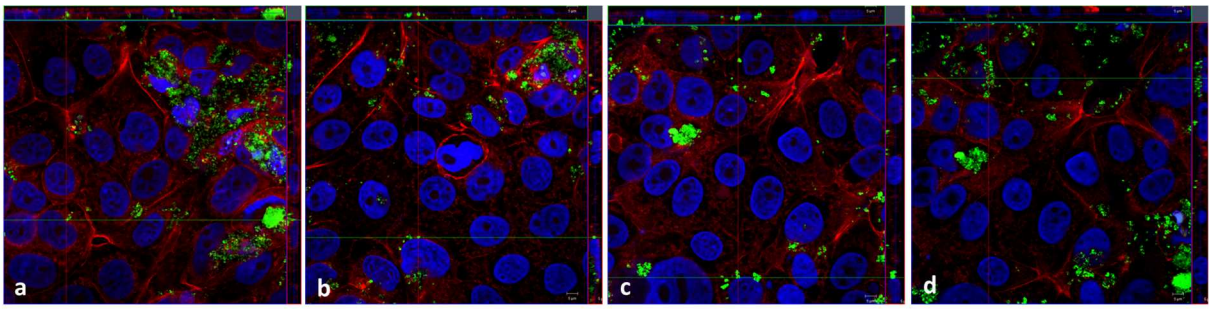

Fig. 8. Confocal microscopy images of $CaCO_3$ NPs intracellular uptake by MCF-7 ((a) image size: 6 µm), SKOV-3 ((b), image size: 8.21 µm), HeLa ((c), image size: 6.91 µm) and CACO-2 ((d), image size: 6.91 µm) cells. Sections of a Z-stack FITC fluorescence (green), phalloidin-TRITC fluorescence and Hoechst-fluorescence-stained nuclei (blue) overlaid images.

3.6 Loading efficiency and release

Drug loading, both on carbonate core naked and functionalized and polymer capsules was calculated by incubating overnight three *cisplatin* solutions with a known concentration (50 μM, 75 μM, 150 μM). As described in the experimental section the supernatant was removed by centrifugation and it was analyzed by ICP. Data analysis of quantitative measurements performed by ICP showed a different behavior comparing the different samples, but the trend stayed the same for all concentrations tested, so the **Fig. 9** shows only the results obtained with the concentration of 150 μM (TEM image in **Fig. SM3**).

The data obtained with naked $CaCO_3$ core, incubated with solutions at different concentrations of *cisplatin* showed the lowest encapsulation efficiency (for the 150 μM solution, loading efficiency of drug on nanocarriers in μg/g ± S.D. 15.8 ± 2). This suggested that the loading of *cisplatin* inside the core did not occur by adsorption in the core interstices due to their porous structure. In fact, functionalizing the surface with silanes chiefly increases the hydrophobicity of the surface. The change in efficiency from APTES to MTMS to MTES was around 25% (loading efficiency respectively 19.5 ± 0.9, 23.9 ± 1.8, and 20.0 ± 3.3 μg/g), confirming that this modification led to a chemical coupling reaction responsible for improved surface interactions. In contrast, the data concerning *cisplatin* loading on DXS/PRM and ALG/PRM capsule showed the highest efficiency, even exceeding 60% in the case of the second pair of polymers tested (loading efficiency 36.7 ± 9.2 and 54.9 ± 6.2 μg/g respectively). Probably, when capsules enter in contact with the solution, the drug is adsorbed onto the capsule surface and into the lumen. The loading efficiency can be influenced by the surface area of the nanoparticles.[47]

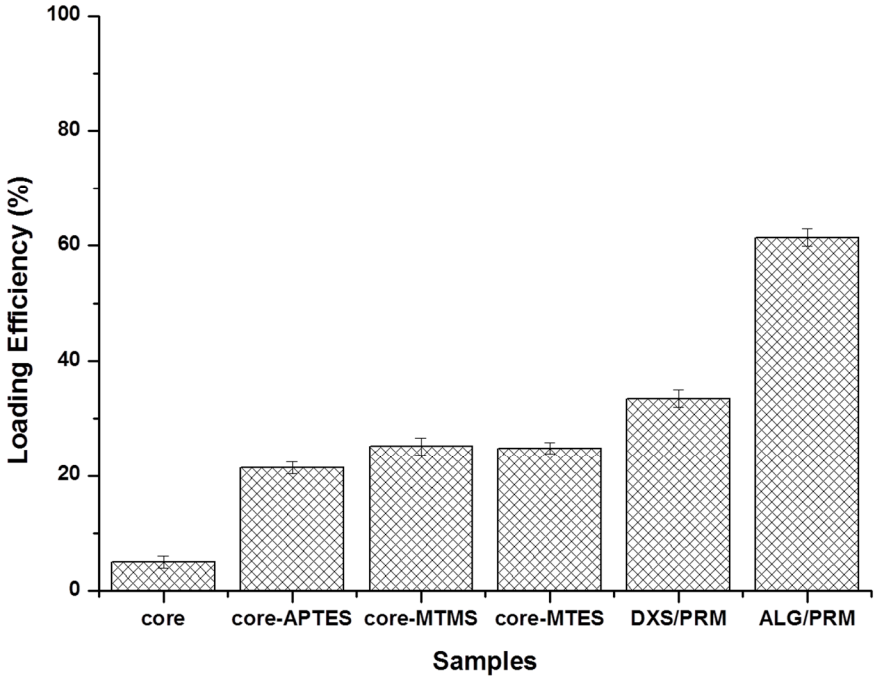

Fig. 9. Relative loading efficiency of *cisplatin* 150μM. Loading efficiency: core 15.8 ± 2.0, APTES 19.5 ± 0.9, MTMS 23.9 ± 1.8, MTES 20.0 ± 3.3 , DXS/PRM 36.7 ± 9.2, ALG/PRM 54.9 ± 6.2 (expressed in μg/g ± S.D.).

The polymeric systems are attractive for their easy tailoring and *in vivo* tolerance, enabling the delivery of various bioactive substances after implantation. Given the good results obtained with polymeric capsules, these were selected for studying both the release of the drug and the effect on a panel of cancer cell lines.

In **Fig. 10**, extended release profile of *cisplatin* from polymeric capsules, with different number of adsorbed layers $(ALG/PRM)_2$ or $(ALG/PRM)_3$, in phosphate buffer saline solution (PBS, pH 7.4) at 37°C are reported. The obtained release profiles indicate sustained manner of drug release from the these polymeric nanocapsules.

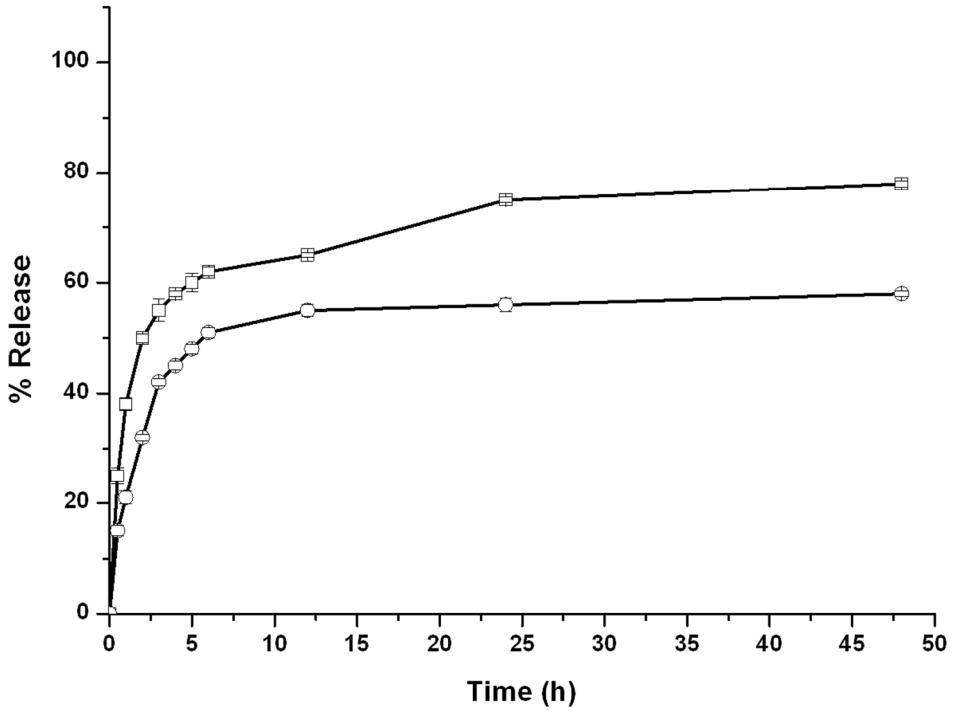

Fig. 10. Controlled *cisplatin* release profiles from the LbL nanocapsules: $(ALG/PRM)_2$ (blue), $(ALG/PRM)_3$ (red).

Controlled release is an attainable and desirable characteristic for a drug delivery systems. The factors affecting the drug release rate revolve around the structure of the matrix containing the drug and the chemical properties associated with both the polymer and the drug. The drug release is also diffusion controlled, as the drug can travel through the pores of polymer shell. The most desirable release profile would show a constant release rate with time. However, in many cases release profiles are more complicated and often contain two main expulsion processes: the first being an initial burst of expelled drug from the shell surface; the second, a usually more constant stage with release rates dependent on diffusion and degradation.

Fig. 10 details the initial burst observed within 60 minutes, followed by a prolonged release. After 48 h a complete release of the drug is still not observed.

LbL technology allows for the easy control of drug release rate from polymer-stabilized colloidal nanoparticles by simple changes of coating thickness or composition.[48] In particular the release curves for *cisplatin* with different coating thickness in standard sink conditions at the same drug concentration of 2 mg/mL were studied. As expected, the release rate was as the number of polyelectrolyte layers in the shell was increased. Certainly, slower release rates are also possible depending on the architecture of the LbL coating.[49]

3.7 Cytotoxicity of loaded nanocapsules

In order to evaluate whether *cisplatin* loaded into the designed nanocarriers exerts cytotoxic effects we carried out an *in vitro* cell viability study, using a panel of four human tumor cell lines, representative of some clinically important types of the neoplastic disease, namely MCF-7 (human breast cancer) SKOV-3 (human ovarian cancer), HeLa (human cervical cancer) and CACO-2 (human epithelial colorectal adenocarcinoma).

In these experiments exponentially growing cells were exposed to two concentrations of free cisplatin 50 and 100μM and its encapsulated formulations $(ALG/PRM)_3$ (0.5 mg) with a nominal drug concentration of approximately 80 μM for 24h.

As expected from the use of concentrations higher than IC_{50},[50-52] chosen to be close to the loading concentrations, the high concentrations of drug used gave minimal difference in viability for the same cell line at the two administered concentrations, with the HeLa cells being more vulnerable to *cisplatin* treatment at higher concentration, in comparison to the other cell lines, as expected for a non-resistant strain (**Fig. 11**).

The higher speed of uptake kinetic compared to the release speed ensures that most of the drug is released after the internalization of the capsules. The loaded nanocarriers afford a decrease in the treated cell viability, close to the one expected for an administration of the free drug at the same nominal concentration. The slightly higher rate of uptake of the nanoparticles in MCF-7 cell line did not translate in an increase in cytotoxicity. Since MCF-7 lines does not

show significant differences from the other cell lines examined in IC_{50} or distribution of nanocapsules, we can assume either a slower or a less efficient degradation pathway in the cell line.

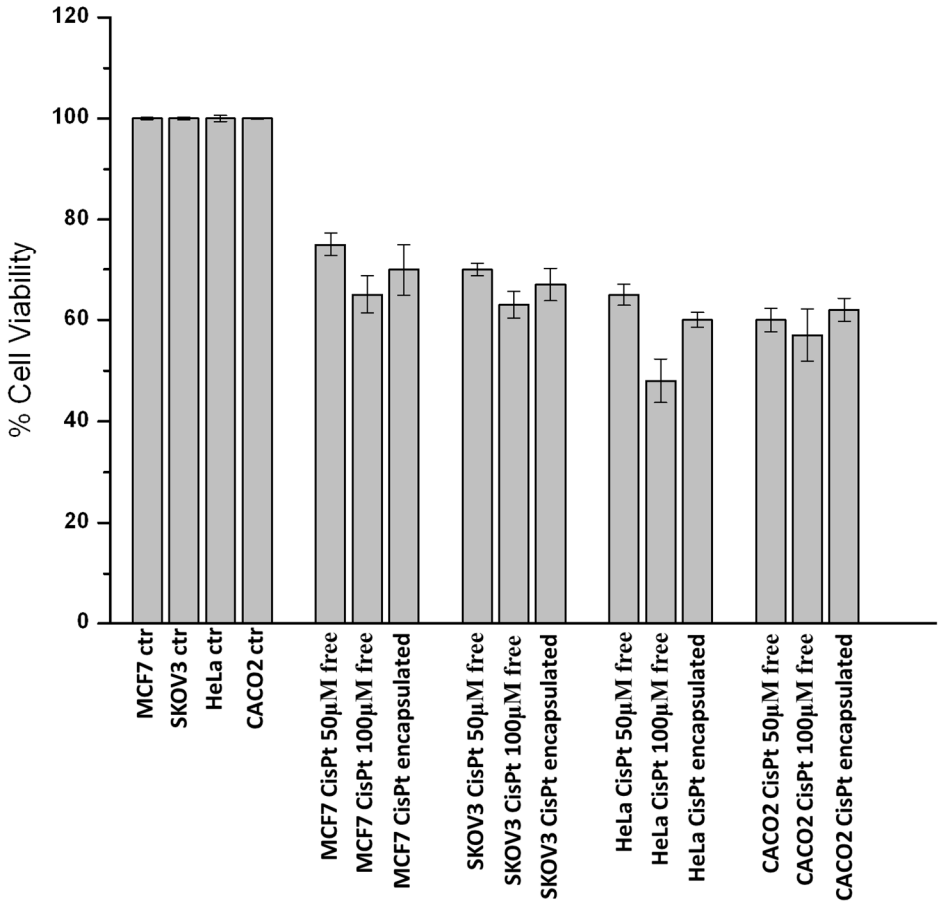

Fig. 11.Fig. Cell viability (% control) of MCF-7, SKOV-3, HeLa and CACO-2 cells treated with 50 and 100 μM of *cisplatin*, and encapsulated formulations $(ALG/PRM)_3$ with a nominal drug concentration of approximately 80 μM. The residual cell number was recorded after 24 h. Data are means ± standard deviations of at least 3 independent replicates.

4. Conclusions

Among the antitumor agents, *cisplatin* [*cis*-diamminedichloroplatinum(II)] is a commonly used drug in the treatment of a variety of solid tumors, usually administered intravenously. A total of 90% of the *cisplatin* is bound to plasma proteins in the blood and, thus, does not enter

the cells; the remaining unbound drug enters the cell as uncharged small molecule. In view of these limitations, research has been extensively focused on drug delivery systems to achieve higher concentration of drug in tumor tissues and controlled release profile for extended time periods.

The development of drug carriers that can improve the water solubility of anticancer drugs and target tumor cells is of high interest for researchers in the field of materials science. Until now, nanocarriers formed by amphiphilic small molecules, block polymers and biomacromolecules have already shown great potential for chemotherapy.[53]

In these report, newly prepared pure nanosized $CaCO_3$ particles, three different types of silane functionalized nano-$CaCO_3$ and LbL synthesized capsules using nano-$CaCO_3$ as template were loaded with *cisplatin*. The loading efficiency on pure nano-$CaCO_3$ cores was very low (below 10%), and while the silanization certainly improved the loading efficiency (around 25% for MTMS and MTES), to improve loading another strategy was attempted, namely the synthesis of LbL capsules of DXS/PRM and ALG/PRM over a nano-$CaCO_3$ core. The best loading was obtained for the ALG/PRM system (over 60%). The capsules with the best loading were then administered to a panel of cell lines, with the objective of evaluating cellular uptake and the activity of the encapsulated drug. The internalization of the coated particles (having the best drug uptake) was fastest on MCF-7 cell lines, showing an uptake close to 75% in 3 hours., but in general, all four cell lines studied showed at least 50% uptake in the first hour of administration. Furthermore, the microscopy studies of FITC showed perinuclear localization of the capsules. The drug release kinetic from the nanocapsules was also studied, showing that the release of the drug takes place at a slower rate than internalization already with the 3 layers capsules. The cytotoxic efficiency of the capsules was comparable to free *cisplatin* at the same nominal concentration for all cell lines. These overall results show that the fabrication of LbL nanocapsules on a nano-$CaCO_3$ shows promise as a drug economic *cisplatin*-delivery system able to release most of its drug load in the

perinuclear area of cancer cells, and moreover the flexibility of the method used leaves ample margins for further tailoring of the carriers.

5. Table of Abbreviations

ALG alginic acid sodium salt

APTES aminopropyltriethoxysilane

$CaCO_3$ calcium carbonate

cisplatin cis-$[PtCl_2(NH_3)_2]$

CLSM confocal laser scanning microscopy

DMSO dimethysulfoxide

DXS dextran sulfate sodium salt

EDTA ethylenediaminetetraacetic acid

ELS electrophoretic light scattering

FBS fetal bovine serum

FITC fluorescein isothiocyanate

GA glutharaldehyde

ICP inductively coupled plasma atomic emission spectroscopy

LDV Laser Doppler Velocimetry

LbL layer by layer

MTES methyltriethoxysilane

MTMS methyltrimethoxysilane

MTT [4,5-dimethylthiazol-2-yl]-2,5- diphenyl tetrazolium bromide

PAH polyallylamine hydrochloride

PDI polydispersity index

PRM protamine sulfate salt

PSS polystyrenesulfonate sodium salt

TEM Transmission Electron Microscopy

Acknowledgements

Financing from University of Salento - Bando «5 PER MILLE PER LA RICERCA» 2012 - Project NanoDEPT, project PON 254/Ric. Potenziamento del "CENTRO RICERCHE PER LA SALUTE DELL'UOMO E DELL'AMBIENTE" Cod. PONa3_00334. CUP: F81D11000210007, and PRIN 2010-2011 (D.M. 1152/ric del 27/12/2011) Nanotecnologie molecolari per il rilascio controllato di farmaci/NANO Molecular tEchnologies for Drug delivery NANOMED prot. 2010FPTBSH, CUP: F81J12000380001 is gratefully acknowledged.

References

[1] H.S. Oberoi, F.C. Laquer, L.A. Marky, A.V. Kabanov, T.K. Bronich, J. Controlled Release, vol. 153, 2011, 64-72.

[2] L. Zhang, F.X. Gu, J.M. Chan, A.Z. Wang, R.S. Langer, O.C. Farokhzad, Clin Pharmacol Ther, vol. 83, American Society of Clinical Pharmacology and Therapeutics, 2007, 761-769.

[3] M.E. Davis, Z. Chen, D.M. Shin, Nat. Rev. Drug Discov., vol. 7, Nature Publishing Group, 2008, 771-782.

[4] V. Vergaro, F. Scarlino, C. Bellomo, R. Rinaldi, D. Vergara, M. Maffia, F. Baldassarre, G. Giannelli, X. Zhang, Y.M. Lvov, S. Leporatti, Adv Drug Deliv Rev, vol. 63, 2011, 847-864.

[5] F. Baldassarre, V. Vergaro, F. Scarlino, F. De Santis, G. Lucarelli, A.D. Torre, G. Ciccarella, R. Rinaldi, G. Giannelli, S. Leporatti, Macromol. Biosci., vol. 12, 2012, 656-665.

[6] V. Vergaro, F. Baldassarre, F. De Santis, G. Ciccarella, G. Giannelli, S. Leporatti, Curr. Pharm. Des., vol. 18, 2012, 4155-4164.

[7] L.L. del Mercato, Adv. Colloid Interface Sci., vol. 207, Elsevier, 2014, 139-154.

[8] V.V. Ciccarella Giuseppe, Leporatti Stefano 2014.

[9] A. Kowalczuk, E. Stoyanova, V. Mitova, P. Shestakova, G. Momekov, D. Momekova, N. Koseva, Int. J. Pharm., vol. 404, 2011, 220-230.

[10] S.E. Sherman, S.J. Lippard, Chem. Rev., vol. 87, American Chemical Society, 1987, 1153-1181.

[11] T.C. Johnstone, J.J. Wilson, S.J. Lippard, Inorg. Chem., vol. 52, American Chemical Society, 2013, 12234-12249.

[12] J.H. Parish, Biochemical Education, vol. 18, Headington Hill Hall, 1990, 157-157.

[13] A.F. LeRoy, R.J. Lutz, R.L. Dedrick, C.L. Litterst, A.M. Guarino, Cancer treatment reports, vol. 63, U.S. Dept. of Health, Education, and Welfare, Public Health Service, National Institutes of Health, 1979, 59-71.

[14] Y. Ohya, S. Shirakawa, M. Matsumoto, T. Ouchi, Polym. Adv. Technol., vol. 11, 2000, 635-641.

[15] J.J. Gullo, C.L. Litterst, P.J. Maguire, B.I. Sikic, D.F. Hoth, P.V. Woolley, Cancer Chemotherapy and Pharmacology, vol. 5, 1980, 21-26.

[16] J.B. Vermorken, W.J.F. Van der Vijgh, I. Klein, Cancer treatment reports, vol. 68, 1984, 505-513.

[17] R.C. DeConti, B.R. Toftness, R.C. Lange, W.A. Creasey, Cancer Res., vol. 33, 1973, 1310-1315.

[18] F. Yu, J. Megyesi, P.M. Price, American Journal of Physiology - Renal Physiology, vol. 295, 2008, F44-F52.

[19] A. Eastman, Cancer Cells, vol. 2, 1990, 275-280.

[20] E.R. Jamieson, S.J. Lippard, Chem. Rev., vol. 99, American Chemical Society, 1999, 2467-2498.

[21] Y. Jung, S.J. Lippard, Chem. Rev., vol. 107, American Chemical Society, 2007, 1387-1407.

[22] B.G. De Geest, N.N. Sanders, G.B. Sukhorukov, J. Demeester, S.C. De Smedt, Chem. Soc. Rev., vol. 36, The Royal Society of Chemistry, 2007, 636-649.

[23] G.B. Sukhorukov, A.L. Rogach, M. Garstka, S. Springer, W.J. Parak, A. Munoz-Javier, O. Kreft, A.G. Skirtach, A.S. Susha, Y. Ramaye, R. Palankar, M. Winterhalter, Small, vol. 3, 2007, 944-955.

[24] C.S. Peyratout, L. Dahne, Angew. Chem. Int. Ed. Engl., vol. 43, 2004, 3762-3783.

[25] G.B. Sukhorukov, A. Fery, M. Brumen, H. Mohwald, PCCP, vol. 6, The Royal Society of Chemistry, 2004, 4078-4089.

[26] B.G. De Geest, S. De Koker, G.B. Sukhorukov, O. Kreft, W.J. Parak, A.G. Skirtach, J. Demeester, S.C. De Smedt, W.E. Hennink, Soft Matter, vol. 5, The Royal Society of Chemistry, 2009, 282-291.

[27] L.J. De Cock, S. De Koker, B.G. De Geest, J. Grooten, C. Vervaet, J.P. Remon, G.B. Sukhorukov, M.N. Antipina, Angew. Chem. Int. Ed., vol. 49, WILEY-VCH Verlag, 2010, 6954-6973.

[28] M. Delcea, A. Yashchenok, K. Videnova, O. Kreft, H. Mohwald, A.G. Skirtach, Macromol. Biosci., vol. 10, 2010, 465-474.

[29] M.F. Bedard, B.G. De Geest, A.G. Skirtach, H. Mohwald, G.B. Sukhorukov, Adv. Colloid Interface Sci., vol. 158, 2010, 2-14.

[30] C.E. Mora-Huertas, H. Fessi, A. Elaissari, Int. J. Pharm., vol. 385, 2010, 113-142.

[31] P.R. Gil, L.L. del Mercato, P. del_Pino, A. Muñoz_Javier, W.J. Parak, Nano Today, vol. 3, 2008, 12-21.

[32] J. Zhang, X.G. Chen, W.B. Peng, C.S. Liu, Nanomed. Nanotechnol. Biol. Med., vol. 4, 2008, 208-214.

[33] S. Mishra, A. Chatterjee, R. Singh, Polym. Adv. Technol., vol. 22, John Wiley & Sons, Ltd., 2011, 2571-2582.

[34] S. Mishra, N.G. Shimpi, A.D. Mali, Polym. Adv. Technol., vol. 23, John Wiley & Sons, Ltd., 2012, 236-246.

[35] J.D. Rodriguez-Blanco, S. Shaw, P. Bots, T. Roncal-Herrero, L.G. Benning, J. Alloys Compd., vol. 536, 2012, S477-S479.

[36] S.-C. Huang, K. Naka, Y. Chujo, Langmuir, vol. 23, American Chemical Society, 2007, 12086-12095.

[37] G. Tari, J.M.F. Ferreira, Ceram. Int., vol. 24, 1998, 527-532.

[38] P. Bertrand, A. Jonas, A. Laschewsky, R. Legras, Macromol. Rapid Commun., vol. 21, WILEY-VCH Verlag GmbH, 2000, 319-348.

[39] S.A. Sukhishvili, Current Opinion in Colloid & Interface Science, vol. 10, 2005, 37-44.

[40] Z. Tang, Y. Wang, P. Podsiadlo, N.A. Kotov, Adv. Mater., vol. 18, WILEY-VCH Verlag, 2006, 3203-3224.

[41] P.T. Hammond, Adv. Mater., vol. 16, WILEY-VCH Verlag, 2004, 1271-1293.

[42] V. Yathindranath, Z. Sun, M. Worden, L.J. Donald, J.A. Thliveris, D.W. Miller, T. Hegmann, Langmuir, vol. 29, American Chemical Society, 2013, 10850-10858.

[43] D. Gibson, Dalton Transactions, The Royal Society of Chemistry, 2009, 10681-10689.

[44] S.J. Lippard, Science, vol. 218, 1982, 1075-1082.

[45] M.D. Hall, M. Okabe, D.W. Shen, X.J. Liang, M.M. Gottesman, Annu. Rev. Pharmacol. Toxicol., vol. 48, 2008, 495-535.

[46] A. Muñoz Javier, O. Kreft, M. Semmling, S. Kempter, A.G. Skirtach, O.T. Bruns, P. del Pino, M.F. Bedard, J. Rädler, J. Käs, C. Plank, G.B. Sukhorukov, W.J. Parak, Adv. Mater., vol. 20, WILEY-VCH Verlag, 2008, 4281-4287.

[47] B.V. Parakhonskiy, A.M. Yashchenok, S. Donatan, D.V. Volodkin, F. Tessarolo, R. Antolini, H. Möhwald, A.G. Skirtach, ChemPhysChem, vol. 15, WILEY-VCH Verlag, 2014, 2817-2822.

[48] I. Marchenko, A. Yashchenok, T. Borodina, T. Bukreeva, M. Konrad, H. Möhwald, A. Skirtach, J. Controlled Release, vol. 162, 2012, 599-605.

[49] A. Agarwal, Y. Lvov, R. Sawant, V. Torchilin, J Control Release, vol. 128, 2008, 255-260.

[50] M. Iafisco, B. Palazzo, G. Martra, N. Margiotta, S. Piccinonna, G. Natile, V. Gandin, C. Marzano, N. Roveri, Nanoscale, vol. 4, The Royal Society of Chemistry, 2012, 206-217.

[51] N. Margiotta, G. Natile, F. Capitelli, F.P. Fanizzi, A. Boccarelli, P. De Rinaldis, D. Giordano, M. Coluccia, J. Inorg. Biochem., vol. 100, 2006, 1849-1857.

[52] N. Kitada, K. Takara, T. Minegaki, C. Itoh, M. Tsujimoto, T. Sakaeda, T. Yokoyama, Cancer Chemotherapy and Pharmacology, vol. 62, Springer-Verlag, 2008, 577-584.

[53] L. Mao, H. Wang, M. Tan, L. Ou, D. Kong, Z. Yang, Chem. Commun., vol. 48, The Royal Society of Chemistry, 2012, 395-397.

$$2NaHCO_3 + CaCl_2 \rightarrow 2NaCl + Ca(HCO_3)_2$$

$$Ca(HCO_3)_2 \rightarrow CaCO_3 + H_2O + CO_2$$

Scheme 1. Chemical reaction

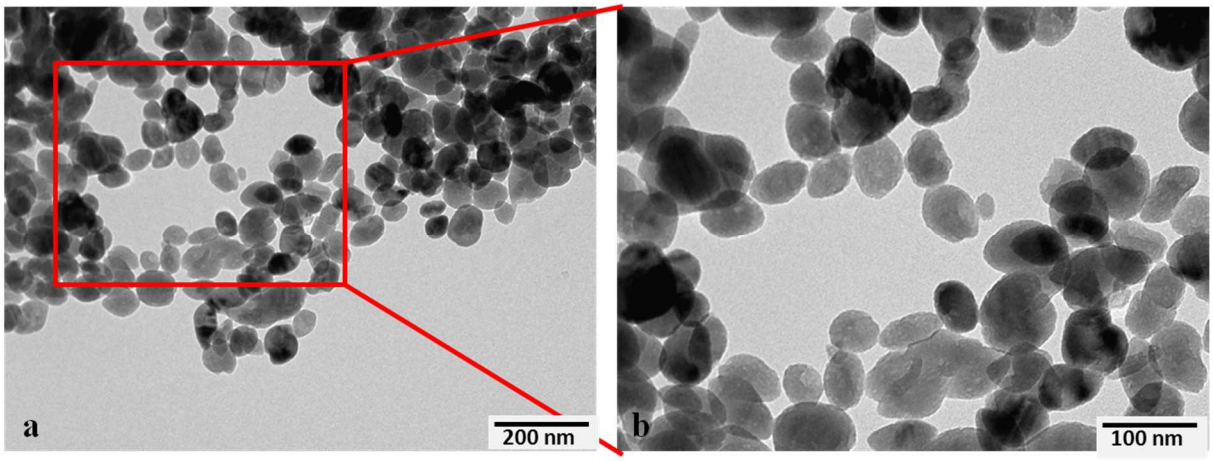

Fig. 1. (a) TEM characterization of nanoCaCO$_3$ nanoparticles, (b) magnification of (a) image.

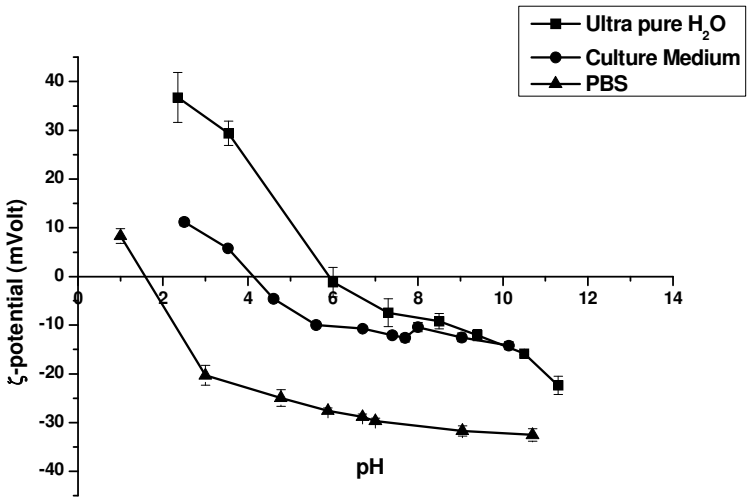

Fig. 2 Variation of ζ-potential of nano-CaCO$_3$ measured in different dispersant: (square) ultra-pure water, (circle) culture media and (triangle) PBS buffer. Averages of 3 separate measurements.

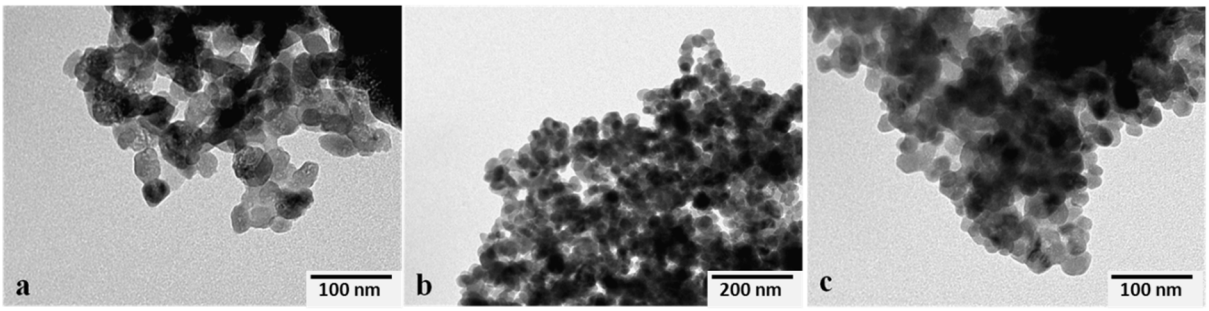

Fig. 3. TEM characterization of $CaCO_3$ nanoparticles after silane modification (a) APTES, (b) MTMS, (c) MTES

Table 1 ζ-potential characterization

Samples	**ζ-value ± SD (mVolt)**
$CaCO_3$	-9.4 ± 1.32
$CaCO_3$ APTES	-18.5 ± 0.6145
$CaCO_3$ MTMS	-20.2 ± 0.87
$CaCO_3$ MTES	-17.5 ± 0.98

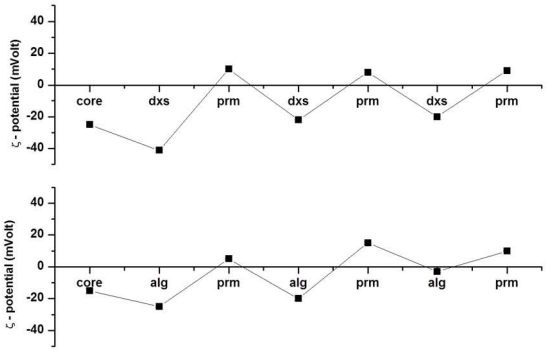

Fig. 4. ζ-potential measurements of two pairs of polyelectrolytes DXS/PRM, ALG/PRM

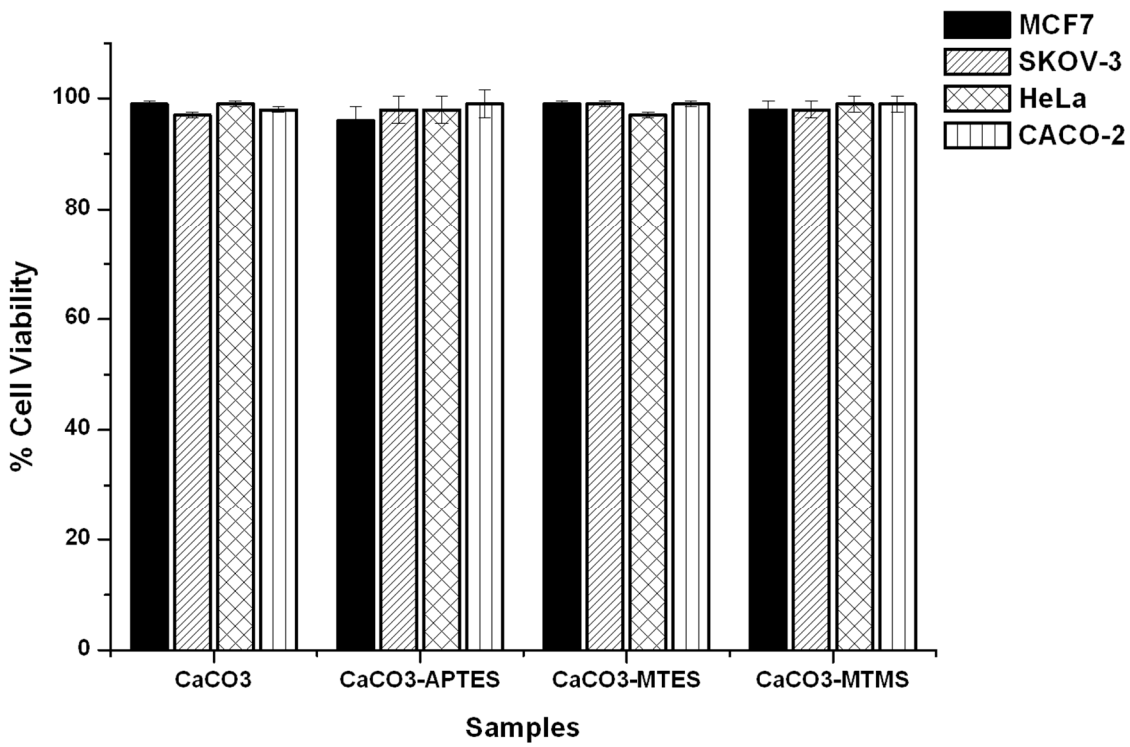

Fig. 5. Cell Viability test performed on MCF7, SKOV-3, HeLa and CACO-2 cell lines incubated for 24h with 1mg/mL of naked $CaCO_3$ or silane functionalized $CaCO_3$.

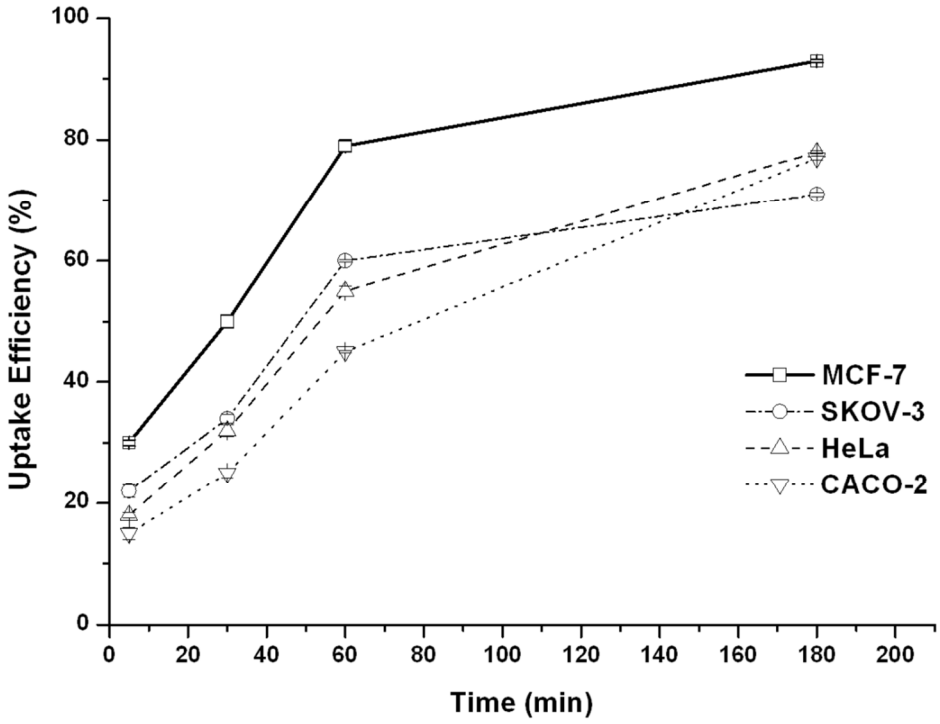

Fig. 6. Kinetics for the uptake of nanoparticles by MCF-7, SKOV-3, HeLa, and CACO-2 cells measured by fluorescence spectroscopy.

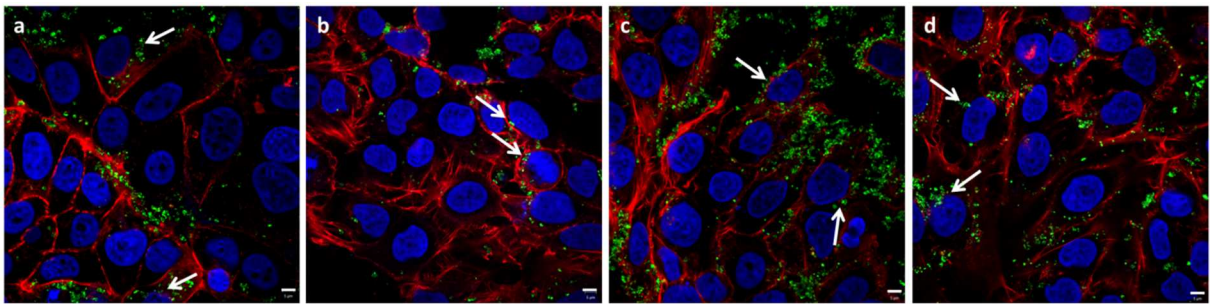

Fig. 7. Confocal microscopy images of nano$CaCO_3$ uptake by MCF-7 (a) SKOV-3 (b), HeLa (c) and CACO-2 (d). In blue are stained nuclei, in red the cytoskeleton (phalloidin-TRITC) and in green nano-$CaCO_3$. Scale bar 5µm.

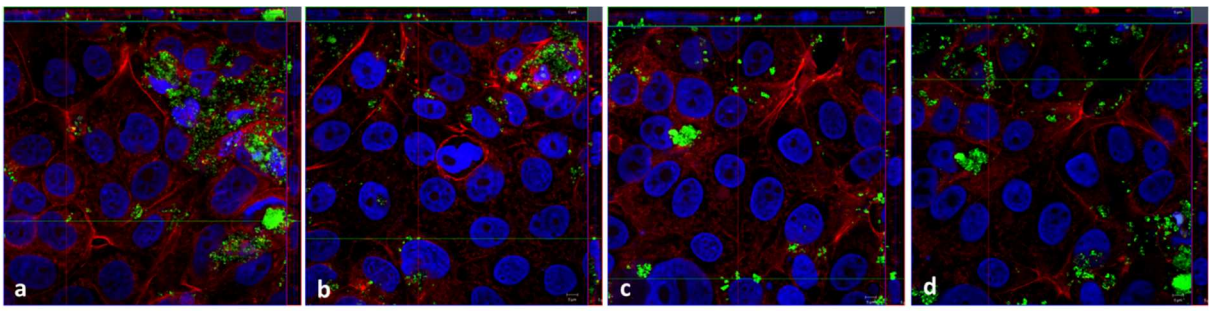

Fig. 8. Confocal microscopy images of $CaCO_3$ NPs intracellular uptake by MCF-7 ((a) image size: 6 μm), SKOV-3 ((b), image size: 8.21 μm), HeLa ((c), image size: 6.91 μm) and CACO-2 ((d), image size: 6.91 μm) cells. Sections of a Z-stack FITC fluorescence (green), phalloidin-TRITC fluorescence and Hoechst-fluorescence-stained nuclei (blue) overlaid images.

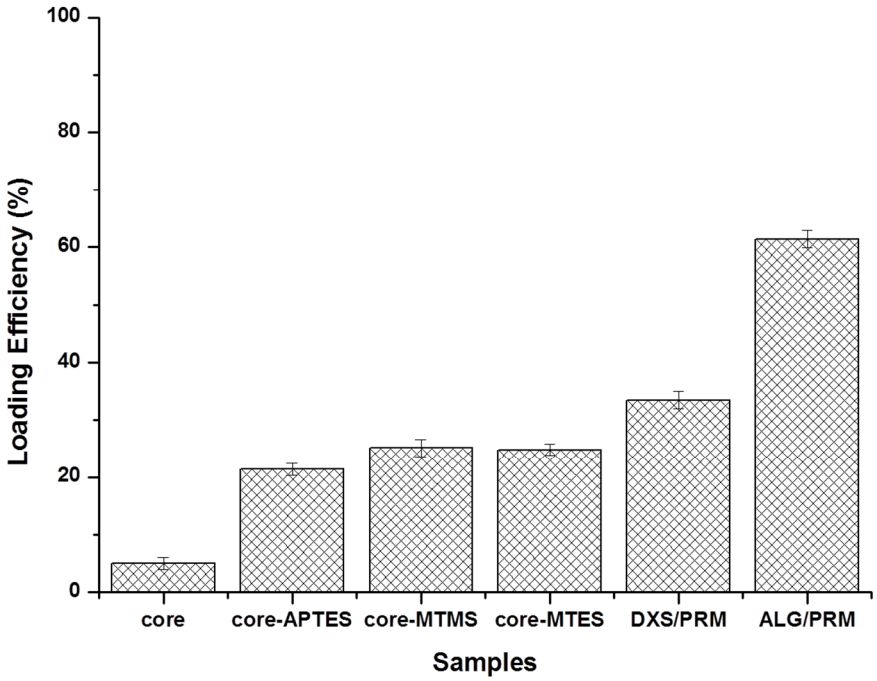

Fig. 9. Relative loading efficiency of *cisplatin* 150μM. Loading efficiency: core 15.8 ± 2.0, APTES 19.5 ± 0.9, MTMS 23.9 ± 1.8, MTES 20.0 ± 3.3 , DXS/PRM 36.7 ± 9.2, ALG/PRM 54.9 ± 6.2 (expressed in μg/g ± S.D.).

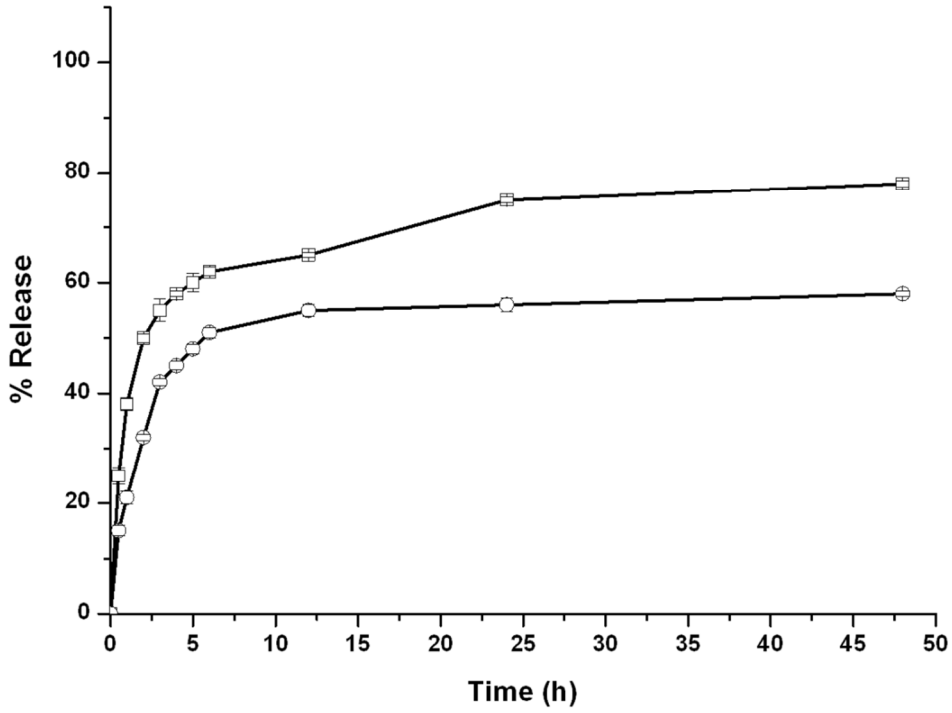

Fig. 10. Controlled *cisplatin* release profiles from the LbL nanocapsules: $(ALG/PRM)_2$ (blue), $(ALG/PRM)_3$ (red).

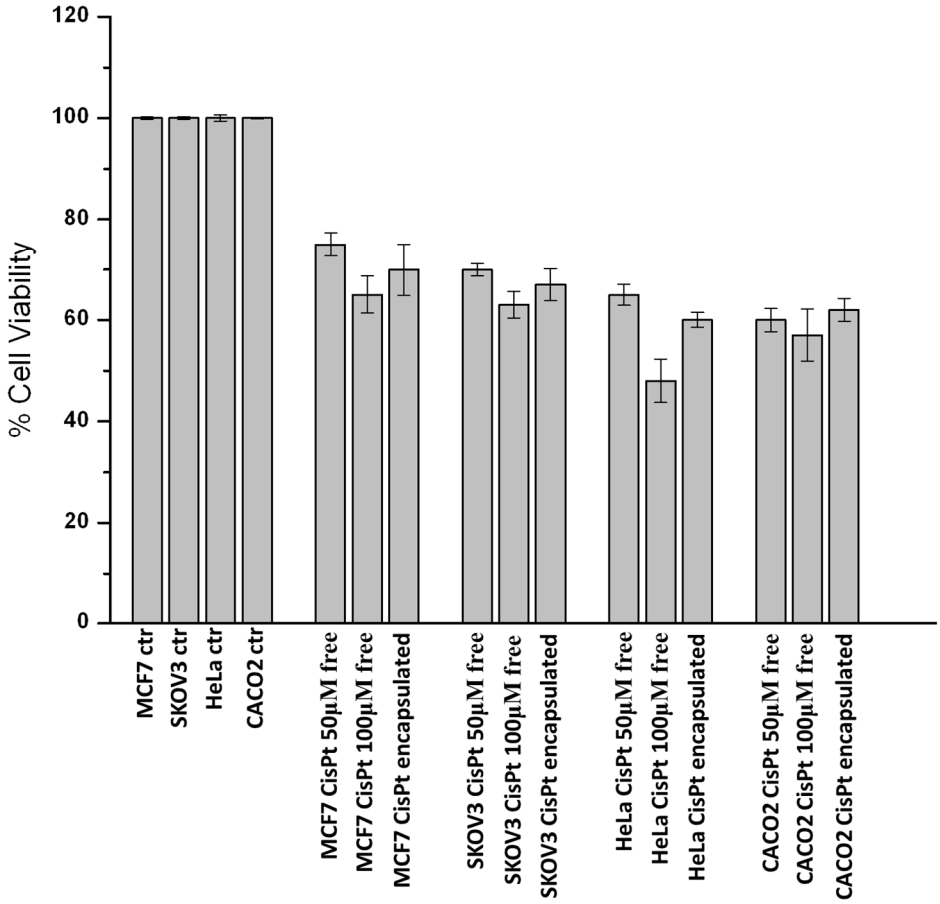

Fig. 11. Cell viability (% control) of MCF-7, SKOV-3, HeLa and CACO-2 cells treated with 50 and 100 μM of *cisplatin*, and encapsulated formulations $(ALG/PRM)_3$ with a nominal drug concentration of approximately 80 μM. The residual cell number was recorded after 24 h. Data are means ± standard deviations of at least 3 independent replicates.